Journal of
Composites Science

MDPI

Article

Support Vector Machine Approach to the Spectroscopic Classification of Archaeological Bitumen Composites in Ancient Mesopotamia

Giulia Festa [1], C. Scatigno [1,*], V. Caruso [1,2], S. Giampaolo [1], A. Tufari [3], L. Ferguson [3], A. Greco [3,4], F. Manclossi [3] and Licia Romano [3]

[1] CREF—Museo Storico Della Fisica e Centro Studi e Ricerche "Enrico Fermi", Via Panisperna 89a, 00184 Rome, Italy; giulia.festa@cref.it (G.F.); caruso.valentina87@gmail.com (V.C.); silvia.giampaolo@cref.it (S.G.)
[2] Dipartimento di Studi Umanistici, Università Degli Studi di Roma Tre, Via Ostiense 236, 00144 Roma, Italy
[3] Dipartimento Istituto Italiano di Studi Orientali, Sapienza Università di Roma, Circonvallazione Tiburtina, 4, 00185 Rome, Italy; tufari.2053996@studenti.uniroma1.it (A.T.); ferguson.2078438@studenti.uniroma1.it (L.F.); greco_angela@hotmail.it (A.G.); francesca.manclossi@gmail.com (F.M.); licia.romano@uniroma1.it (L.R.)
[4] Gerda Henkel Stiftung, Malkastenstraße 15, 40211 Düsseldorf, Germany
* Correspondence: claudia.scatigno@cref.it

Abstract

In ancient civilisations, bitumen was widely used for its multifunctional applications in construction, sealing, and adhesion, evidencing early expertise in material engineering and resource optimisation. Here, Sumerian bitumen-based artefacts were studied through Fourier transform infrared spectroscopy (FTIR) and machine learning to investigate ancient practices for the repair, reuse, and recycling of everyday materials. The materials are dated back to the 3rd millennium BC and come from the archaeological site of Abu Tbeirah (Iraq). Four primary classes were identified based on their molecular composition, which revealed a specific gradient determined by the varying proportions of bitumen and other fillers. These composition-based classes were then applied to predict the classification of the undetermined samples, which constitute 50% of the entire dataset, via a kernel-based support vector machine (SVM). The new findings are consistent with philological sources that reference distinct formulations of use in everyday life. The findings offer a new perspective on the social and historical importance of the circular economy.

Keywords: Sumerian bitumen; spectroscopic features; machine learning

Academic Editor: José António Covas

Received: 28 August 2025
Revised: 16 October 2025
Accepted: 27 October 2025
Published: 2 November 2025

Citation: Festa, G.; Scatigno, C.; Caruso, V.; Giampaolo, S.; Tufari, A.; Ferguson, L.; Greco, A.; Manclossi, F.; Romano, L. Support Vector Machine Approach to the Spectroscopic Classification of Archaeological Bitumen Composites in Ancient Mesopotamia. *J. Compos. Sci.* **2025**, *9*, 596. https://doi.org/10.3390/jcs9110596

1. Introduction

Bitumen-based materials were widely used for practical purposes in Sumerian civilisation, such as waterproofing, construction, and as adhesives [1–3]. Thanks to its intrinsic physical and chemical characteristics, Bitumen was suitable for a large variety of applications such as mortar components in brick buildings, as adhesive for repairing objects, and as sealing products [4–6]. It is highly viscous at room temperature, but its viscosity decreases significantly with increasing temperature, making it more fluid and workable when heated. To enhance its performance, ancient users frequently modified its rheological (e.g., viscosity and flexibility) and mechanical (e.g., strength and durability) properties by incorporating various fillers such as mineral aggregates (i.e., gravels and sands) and organic materials (i.e., straw and natural fibres) [7,8]. In some cases, more sophisticated modifications included

the addition of waxes, oils, and resins, which could lower the melting point of the mixture, thereby saving fuel and time during processing and application.

These technical variations acquire further significance when considered against the background of environmental and economic constraints. Primary resources in the Sumerian region such as wood, stones, and metals were not locally available and had to be acquired through commerce. Bitumen, although sourced from relatively nearby areas, was nonetheless considered a primary resource of considerable value. Its strategic role in various production processes made it a frequent candidate for reuse and recycling, reflecting broader patterns of resource optimisation in the Sumerian economy.

The study presented here has been carried out within the framework of the SLOW SUMER project [9] which contributes to a comprehensive analysis of the practices of repairing, reusing, and recycling everyday materials, with the aim of exploring how societies past managed and extended the lifecycle of their material resources—particularly during the period of 2500–2000 BCE, a time marked by significant political, cultural, and environmental changes. A specific focus of the project is the reconstruction of the lifecycle and recycling trajectories of bitumen in third-millennium BCE southern Mesopotamia. In particular, the project investigates ancient practices related to the procurement, handling, processing, and storage of bitumen, as well as the methods employed for its reuse and recycling in domestic contexts. In order to reconstruct the chaîne opératoire and recycling trajectories of bitumen, the project incorporates scientific techniques commonly used in materials analysis. In recent years, machine learning (ML) has been successfully applied in chemistry to interpret patterns in spectroscopic data [10–13] analysing large amounts of information generated by different techniques such as infrared spectroscopy [14–16], X-ray fluorescence spectroscopy (XRF) [17,18], mass spectrometry [19–21], extracting meaningful insights from complex datasets. The application of ML was also successfully integrated into heritage science, demonstrating its efficacy across various domains such as the classification of artefacts, digital reconstruction of damaged cultural heritage objects, and predictive analysis in the context of cultural heritage preservation [22–26].

Here, Fourier transform infrared spectroscopy (FTIR) combined with machine learning was used to examine the spectroscopic features of bitumen-based materials from the archaeological site of Abu Tbeirah [27–30], which dates to the second half of the third millennium BCE. This medium-sized Sumerian settlement, located near the city of Ur and formerly situated along the shoreline of the ancient Gulf, has yielded a range of archaeological contexts through recent excavations. Among the most significant discoveries is a large domestic complex of approximately 600 square metres (Building A). This exceptional find offers, for the first time, a detailed window into the daily life of non-elite communities during the 3rd millennium BCE—a perspective undocumented in the contemporary written record. Although cuneiform sources from this period are abundant, they overwhelmingly reflect the activities of elite administrative institutions, thus limiting our understanding of broader societal practices. Within this domestic context, evidence of a bitumen workshop was identified, presenting a rare opportunity to investigate the use, reuse, and recycling of bitumen among commoners. This allows for a comparative analysis between archaeological data and the administrative narratives preserved in cuneiform texts, shedding light on material practices that would otherwise remain undocumented.

2. Materials and Methods

2.1. Materials

A set of 60 bitumen samples from the archaeological site of Abu Tbeirah were investigated and reported in Figure 1. Two reference standards, soil from the excavated archaeological contexts and modern bitumen, were analysed for comparative purposes.

Samples were polished on the surface, and a clean cross-section was prepared to minimise the effect of soil contamination. Due to the complex structure of the samples, including the presence of mineral and vegetal inclusions, FTIR measurements were carried out on selected areas of the bituminous matrix. Micro-sampling was carried out following surface cleaning procedures to minimise signal interference from soil contamination and ensure the representativeness of the analytical measurements. The samples were initially classified based on their contextual and archaeological information as reported in Table 1.

Based on both their archaeological context and observable morphological characteristics, we propose a preliminary classification. The following categories and subcategories, as reported in Table 1, were identified through macroscopic observations:

(a) Ingots: samples shaped with one convex and one flat side, with the latter often bearing impressions of woven mats and having a flat shape with one convex side (i.e., samples 6, 35, 42, 44, and 46). These artefacts are interpreted as transport units [31].

(b) Traces: samples where bitumen is present only as a minor or incidental component, indicating secondary or auxiliary uses, including the following:
(b_1) Adhesive materials: samples that include bitumen used as glue, for instance in the construction of sickles (i.e., samples 1, 37, and 47), or as an adhesive for repairs, such as sample 43, which was used to bond parts of a sarcophagus found in Grave 17.
(b_2) Residues of bitumen found in association with objects (i.e., sample 21 on grinding stone, sample 41 in which bitumen was used for waterproofing containers woven from vegetal fibres, and sample 60 on pottery).
(b_3) Traces on grindstones are hypothesised to be remnants of bitumen processing activities, while residues on pottery may indicate the use of ceramic vessels within the bitumen processing workflow.

(c) Spherical artefacts: this category comprises bitumen objects characterised by a rounded morphology, including the following:
(c_1) Rounded artefacts: samples that have a rounded shape.
(c_2) Perforated artefacts: samples featuring a central hole (i.e., samples 28, 30, 33, and 55).
(c_3) Drop-shaped artefacts: samples that have a distinctive drop shape (i.e., samples 2, 9, 22, 23, 32, 34, and 36). They may represent intermediate storage forms of bitumen, possibly intended for later reuse within ongoing recycling processes. Indeed, they were found grouped within the workshop area of Abu Tbeirah.

(d) Undetermined artefacts: This category comprises bitumen objects whose function remains unclear, lacking distinctive features allowing for specific functional identification:
(d_1) Undetermined: without a specific shape or distinguishing feature
(d_2) Flat fragments: samples that have a flat shape and currently unidentifiable function (i.e., samples 10, 19, 38, 39, 51, and 52). Although the function is unknown, they constitute a specific macroscopic category based on distinct morphological traits.

Approximately 30% of the samples are labelled as "undetermined", as their shape does not allow for a definitive assignment of function or classification, thereby preventing the determination of their specific usage type. As these samples comprise a substantial part of the archaeological assemblage, the accurate attribution of these fragments is highly important. These are crucial pieces of evidence, as they most likely formed part of the bitumen recycling chain, indicating their direct involvement in everyday practices of material reuse.

Table 1. List of the samples analysed.

ID	Label	Excavation Campaign	Area	Context Type	Context	Phase	Room	Grave	US	Inv. No.	Preservation	Category	Short Description
SlS_07	1	2017	4	Domestic	Building D	2	-	-	1134	AbT.17.121	Residue	Adhesives	Flint blade with bitumen haft
SlS_08	2	2015	1	Domestic	Building A	1	16	-	358	AbT.15.71	Complete	Dropped object	Dropped object
SlS_09	3	2017	6	Domestic	Building E 2	-	-	-	1544	AbT.17.114	Fragments	Undetermined	Fragments of bitumen object
SlS_10	4	2015	1	Domestic	Building A	1	2	-	397	AbT.15.108 A	Fragment	Undetermined	Bitumen fragment
SlS_11	5	2015	1	Workshop	Building A	1	23	-	395	AbT.15.125	Fragments	Undetermined	Bitumen objects (3 fragments)
SlS_12	6	2015	1	Domestic	Building A	1	18	-	381	AbT.15.86	Fragments	Ingot	Various bitumen fragments of ingot
SlS_13	7	2017	4	Domestic	Building D	-	5	-	1111	AbT.17.32	Fragments	Undetermined	Bitumen object (3 fragments)
SlS_14	8	2017	4	Domestic	Building D	-	5	-	1111	AbT.17.34	Fragments	Undetermined	Bitumen object with a small hole
SlS_16	9	2015	1	Domestic	Building A	1	18	-	381	AbT.15.89	Fragment	Dropped object	Dropped object
SlS_17	10	2013	2	Funerary	Cemetery	-	-	102	585	AbT.13.65	Fragments	Flat fragments	Bitumen object
SlS_18	11	2015	1	Workshop	Building A	1	23	-	-	AbT.15.123	Complete	Rounded object	Spherical bitumen object
SlS_19	12	2016	4	Surface	Building D	-	-	-	1013	AbT.16.72	Fragments	Undetermined	Fragments of bitumen and soil
SlS_20	13	2015	1	Workshop	Building A	1	23	-	419	AbT.15.138	Complete	Undetermined	Bitumen object
SlS_21	14	2015	1	Domestic	Building A	1	14	-	338	AbT.15.33	Fragment	Undetermined	Bitumen object
SlS_22	15	2017	4	Domestic	Building D	-	5	-	1111	AbT.17.31	Fragment	Undetermined	Bitumen object

Table 1. *Cont.*

ID	Label	Excavation Campaign	Area	Context Type	Context	Phase	Room	Grave	US	Inv. No.	Preservation	Category	Short Description
SlS_23	16	2017	1	Domestic	Building A	2	23	-	634	AbT.17.9	Fragments	Undetermined	Bitumen object fragmented
SlS_24	17	2015	1	Domestic	Building A	1	16	-	358	AbT.15.47	Fragments	Undetermined	Various bitumen fragments
SlS_25	18	2017	1	Domestic	Building A	2	23	-	634	AbT.17.21	Fragment	Undetermined	Bitumen object
SlS_26	19	2017	4	Domestic	Building D	-	5	-	1111	AbT.17.33	Fragment	Flat fragments	Bitumen object
SlS_27	20	2017	4	Domestic	Building D	-	5	-	1111	AbT.17.31	-	Undetermined	Bitumen object
SlS_28	21	2015	1	Domestic	Building A	1	16	-	358	AbT.15.46	Residue	Residue on grindstone	Grindstone with traces of bitumen
SlS_29	22	2017	1	Domestic	Building A	2	23	-	634	AbT.17.6	Complete	Dropped object	Dropped object
SlS_30	23	2017	1	Domestic	Building A	2	23	-	634	AbT.17.7	Fragment	Dropped object	Dropped object
SlS_31	24	2015	1	Domestic	Building A	1	14	-	338	AbT.15.37	Fragment	Undetermined	Bitumen object
SlS_32	25	2017	6	Surface	Surface	-	-	-	1503	AbT.17.56	Fragment	Undetermined	Bitumen fragment
SlS_33	26	2017	6	Domestic	Building E 2	-	-	-	1505	AbT.17.51	Fragments	Vessel	Fragments of bitumen object
SlS_34	27	2017	1	Domestic	Building A		14 (out)	-	631	AbT.17.27	Fragments	Undetermined	Fragments of bitumen object
SlS_35	28	2015	1	Domestic	Building A	2	2	-	409	AbT.15.113	Fragment	Perforated object	Spherical bitumen object
SlS_36	29	2015	1	Domestic	Building A	1	22	-	394	AbT.15.143	Fragments	Undetermined	Various bitumen fragments
SlS_37	30	2017	1	Domestic	Building A	2	23	-	634	AbT.17.8	Fragment	Rounded object	Bitumen fragment of object
SlS_38	31	2015	1	Domestic	Building A	1	2	-	397	AbT.15.108B	Fragment	Undetermined	Bitumen fragment

Table 1. *Cont.*

ID	Label	Excavation Campaign	Area	Context Type	Context	Phase	Room	Grave	US	Inv. No.	Preservation	Category	Short Description
SlS_39	32	2017	1	Domestic	Building A	2	23	-	634	AbT.17.10	Fragment	Dropped object	Dropped object
SlS_40	33	2015	1	Domestic	Building A	1	14	-	338	AbT.15.30a	Complete	Rounded object	Two bitumen objects
SlS_41	34	2017	1	Domestic	Building A	2	23	-	634	AbT.17.5	Fragment	Dropped object	Bitumen object
SlS_42	35	2017	6	Domestic	Building E 2	-	-	-	1505	AbT.17.52	Fragments	Ingot	Fragments of bitumen object
SlS_43	36	2016	1	Domestic	Building A	2	10	-	434	AbT.16.6	Complete	Dropped object	Dropped object
SlS_44	37	2016	1	Domestic	Building A	2	9	-	489	AbT.16.68	Residue	Adhesives	Flint bladelet
SlS_45	38	2017	1	Domestic	Building A	2	14–15	-	657	AbT.17.80	Fragment	Flat fragments	Bitumen object
SlS_46	39	2015	1	Domestic	Building A	1	17+19 +21	-	379	AbT.15.78	Fragment	Flat fragments	Bitumen fragments
SlS_48	40	2015	1	Funerary/ Workshop	Cemetery	-	-	24	365	-	-	Adhesives	-
SlS_49	41	2015	1	Workshop	Building A	1	23	-	395	AbT.15.395.7	Residue	Residue on pottery	Residue inside jar
SlS_50	42	2014	1	Domestic	Building A	2	5	-	222	-	Fragment	Ingot	Fragment of ingot
SlS_51	43	2014	1	Funerary	Cemetery	-	-	17		-	Residue	Adhesives	Glueing together sarcophagus
SlS_52	44	2013	1	Funerary	Cemetery	-	-	16	195	-	Fragment	Ingot	-
SlS_53	45	2015	1	Funerary/ Workshop	Cemetery	-	-	24	372	-	Residue	Undetermined	-
SlS_54	46	2014	1	Domestic	Building A	2	4	-	126	-	Complete	Ingot	Bitumen ingot

Table 1. *Cont.*

ID	Label	Excavation Campaign	Area	Context Type	Context	Phase	Room	Grave	US	Inv. No.	Preservation	Category	Short Description
SlS_55	47	2015	1	Workshop	Building A	1	23	-	395	AbT.15.114	Residue	Adhesives	Bitumen sample on sickle blade
SlS_57	48	2015	1	Workshop	Building A	1	23	-	395	AbT.15	Residue	Undetermined	Bitumen fragment
SlS_58	49	2015	1	Funerary/ Workshop	Cemetery	-	-	24	365	AbT.24.1	Fragments	Vessel	Bitumen fragments
SlS_59	50	2015	1	Funerary/ Workshop	Cemetery	-	-	24	365	AbT.24.2	Fragments	Undetermined	Bitumen fragments
SlS_60	51	2015	1	Funerary/ Workshop	Cemetery	-	-	24	365	AbT.24.3	Fragment	Flat fragments	Bitumen fragment with impression
SlS_61	52	2015	1	Funerary/ Workshop	Cemetery	-	-	24	365	AbT.24.4	Fragment	Flat fragments	Bitumen fragment
SlS_62	53	2015	1	Funerary/ Workshop	Cemetery	-	-	24	365	AbT.24.5	Fragments	Undetermined	Bitumen fragments
SlS_63	54	2015	1	Funerary/ Workshop	Cemetery	-	-	24	365	AbT.24.6	Fragments	Undetermined	Bitumen fragments
SlS_64	55	2015	1	Funerary/ Workshop	Cemetery	-	-	24	365	AbT.24.7	Fragment	Perforated object	Bitumen fragment
SlS_65	56	2017	4	Domestic	Building D	-	5	-	1113	AbT.17.95	Complete	Reed basket	Reed basket
SlS_66	57	2015	1	Workshop	Building A	1	23	-	395	-	Residue	Undetermined	-
SlS_67	58	2017	1	Domestic	Building A	2	14–15	-	659	-	Residue	Residue on pottery	Bitumen incrustation on pottery
SlS_68	59	2013	1	Domestic	Building A	2	4	-	136	AbT.24.8	Fragments	Undetermined	Bitumen object(s)
SlS_69	60	2017	4	Domestic	Building D	-	6&7&8	-	1120	AbT.24.9	Fragments	Undetermined	Bitumen object(s)
soil	61	-	-	-	-	-	-	-	-	-	-	-	-
STD bitumen	62	-	-	-	-	-	-	-	-	-	-	-	

Figure 1. Analysed samples.

2.2. Fourier Transform Infrared Spectroscopy (FTIR) Investigations

FTIR spectra were acquired using a NICOLET™ iS5 spectrometer (Thermo Scientific™, Waltham, MA, USA) [32] equipped with a DTGS detector and a KBr beam splitter. Measurements were performed in ATR mode (T%) over the 4000–400 cm^{-1} range, with 128 scans per spectrum at a resolution of 2 cm^{-1}. A total of 62 spectra were collected under the same experimental conditions to ensure reproducibility. Spectral processing and visualisation were carried out using OMNIC™ and OriginPro® 2021 (OriginLab Corp., Northampton, MA, USA) [33].

2.3. Supervised Machine Learning Model

A supervised classification approach was employed, integrating a support vector machine (SVM) with principal component analysis (PCA), to discriminate archaeological bitumen samples based on their spectral signatures. PCA was initially applied as a dimensionality reduction technique. The first five principal components were retained to project the high-dimensional spectral data into a lower-dimensional space and to facilitate residue analysis. This facilitated the classification process and enabled the assignment of predicted classes to undetermined bitumen samples.

Data Loading and Preprocessing. Each spectrum is assigned a label following the archaeological bitumen sample assignments that were initially classified based on their archaeological context and macroscopic characteristics. These include, for instance, adhesives, residues, ingots, and other functional forms, as outlined in previous paragraphs These labels serve as ground truth for supervised learning. Spectra labelled as "Undetermined" were treated as unknown data during model training and were used in the prediction phase.

SVM Model Training. A machine learning model was constructed to classify the bitumen samples based on their spectral profiles. It consists of a standard scaler for feature normalisation, followed by a support vector classifier (SVC) with a radial basis function (RBF) kernel, which is well suited for handling high-dimensional and non-linearly separable data. The classifier was trained exclusively on the spectra associated with labelled samples, leveraging the known archaeological classes to learn patterns in the spectroscopic data. Once the model was trained, it was applied to the "Undetermined" test samples to predict their most likely class labels. In addition to the predicted label, the model outputs a class probability distribution, representing the confidence of the prediction across all defined classes.

The workflow for this study is presented in Figure 2.

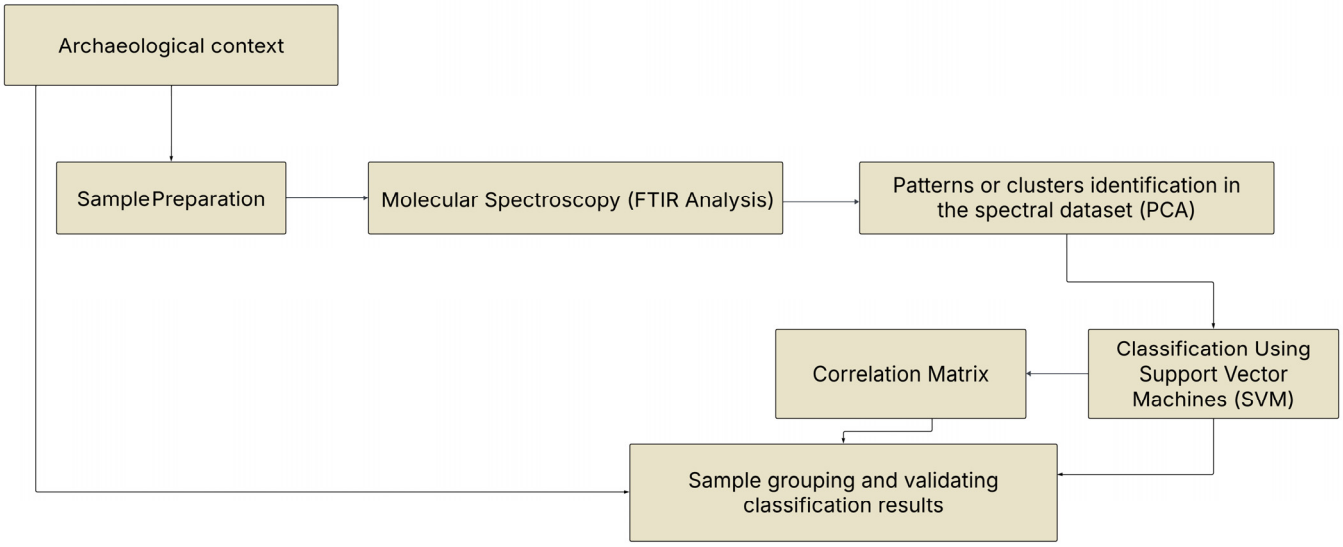

Figure 2. Workflow of the present study.

3. Results and Discussion

To investigate the chemical composition, preservation state, and potential additives of archaeological bitumen, FTIR spectra were acquired for a total of 60 archaeological samples, with one soil sample from the excavation and one modern bitumen sample used as references. Variations in the FTIR spectra serve as key indicators of chemical differences, linked to usage conditions, degrees of alteration, or the deliberate addition of fillers or tempering agents. Representative spectra, one for each main macroscopic category observed, is presented in Figure 3. The modern bitumen sample in Figure 3 displays the typical absorption bands of hydrocarbon-based materials, with signals from alkyl functional groups. These are characteristics of a well-preserved bitumen matrix and serve as a reference for comparison with the archaeological ones. In contrast, the excavation soil shows strong bands associated with carbonates and silicates due to its mineral composition. Archaeological bitumen samples show different ratios of organic/inorganic content—for instance, in the region between 1200 and 1800 cm^{-1}—and characteristic spectra features such as bands associated with alkyl functional groups like $_{sym.\&asym}$.CH, -CH_2, and -CH_3, which are typical of hydrocarbons.

Principal component analysis (PCA) was carried out to identify compositional trends and patterns. The dataset is composed of 62 spectra, resulting in a matrix of shape 62 × 14,935. The PCA was computed using a mean-centred approach with the non-iterate singular value decomposition algorithm and cross-validation method, and results are reported in Figure 4. The loadings plot is used to identify the components that significantly describe the system. Based on this analysis, we selected up to the fifth PC with the following explained variance PC1—64.4%, PC2—15.3%, PC3—5.9%, PC4—3.4%, and PC5—2.7%, accounting for a cumulative variance of approximately 92%.

In Figure 4a, scores plots for PC1 and PC2 are shown and describe the data structure in terms of overarching sample patterns. A specific pattern is identified at PC1 > 0 and PC2 > 0 for samples 22, 41, 48, and 57, which cluster in proximity to the soil reference sample n. 61. These samples are characterised by high signals from carbonates and silicates. Sample 22 corresponds to a drop-shaped bitumen object, sample 41 comes from residues recovered from the internal area of a jar, while sample 48 has an undetermined origin and was found among the remains of a jar, showing a high degree of soil contamination. On the other hand, in the region defined by PC1 < 0 and PC2 > 0, a distinct cluster includes samples n. 1, 3, and 5. Sample 1 was recovered from the bituminous adhesive employed to attach a

now-lost handle (possibly made of a perishable material) to the chert blade, likely serving as part of a hafting or binding system, while sample 3 is identified as undetermined. The sample closest to the modern and pure bitumen reference (sample n. 64) is the sample n. 43, which is described as an adhesive to repair a sarcophagus. Samples identified as ingots through macroscopic observations are in the PC1 < 0 region, not far from the bitumen reference sample. An analysis of the sample distribution in the PCA score plot indicates that PC1 accounts for the main variance among the data and is associated with bitumen ageing, whereas the variance along PC2 is linked to contamination, such as the presence of additives and fillers.

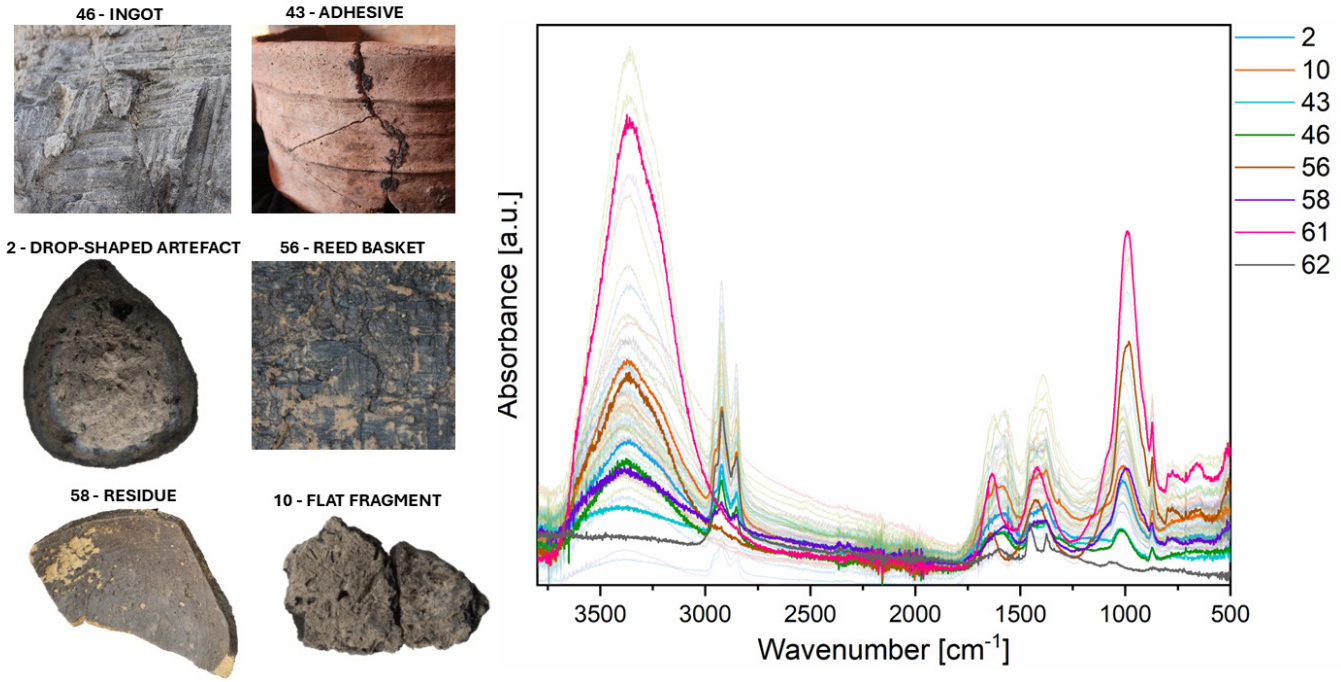

Figure 3. Some selected images and the FTIR spectra dataset. The spectra are shown with transparency to highlight overlapping peaks. Sample 2 (sky-blue) corresponds to bitumen with a distinctive drop shape; sample 10 (orange) refers to a bitumen fragment with a flat shape; sample 43 (turquoise) corresponds to the bitumen used as an adhesive to repair a ceramic sarcophagus; sample 46 (green) is a bitumen fragment coming from an ingot; sample 56 comes from a reed basket coated with bitumen; and sample 58 is a bituminous residue on a pottery vase. Samples 61 and 62 correspond, respectively, to the excavation soil and a modern bitumen standard used as references.

Figure 4b reports the loading plot for the five principal components. The main IR absorption bands characterising the dataset are indicated with dashed lines and listed in Table 2. The plot shows spectral regions which contribute most to the discrimination of bitumen samples along each principal component.

Table 2. List of IR absorption bands which characterise the dataset and are reported in the loading plot in Figure 4.

Wavenumber [cm^{-1}]	Assignment	Vibrational Mode	References
3300–3400	Hydrogen-bonded –OH (resins, asphaltenes, and oxidation products)	νO-H	[34–36]
2952, 2920, 2850, 1380, 720	Aliphatic chains (resins and saturates)	$\nu_{sym\&asym}$ CH	[34,35,37,38]
1490, 1455, 1425, 1380	Aliphatic deformation	νCH_2, δCH_3	[35–38]
1600	Aromatic C–H and C=C from asphaltenic fraction	νC–H, νC=C	[35,36]
1640	Conjugated ring vibration	C=C	[35,37–39]
1700	Carbonyl groups (aged bitumen)	νC=O	[34,39]

Table 2. *Cont.*

Wavenumber [cm^{-1}]	Assignment	Vibrational Mode	References
1310, 1160	Sulfones	$\nu_{sym\&asym}$ S=O	[35,39–41]
1057	Silicate mineral contamination, fillers	νSi-O	[42]
1030	Sulfoxides (aged bitumen)	νS=O	[34,36–39,43]
1057, 875	Carbonate minerals, contamination, and fillers	δCO_3^{2-} out-of-plane, Si-O	[44]

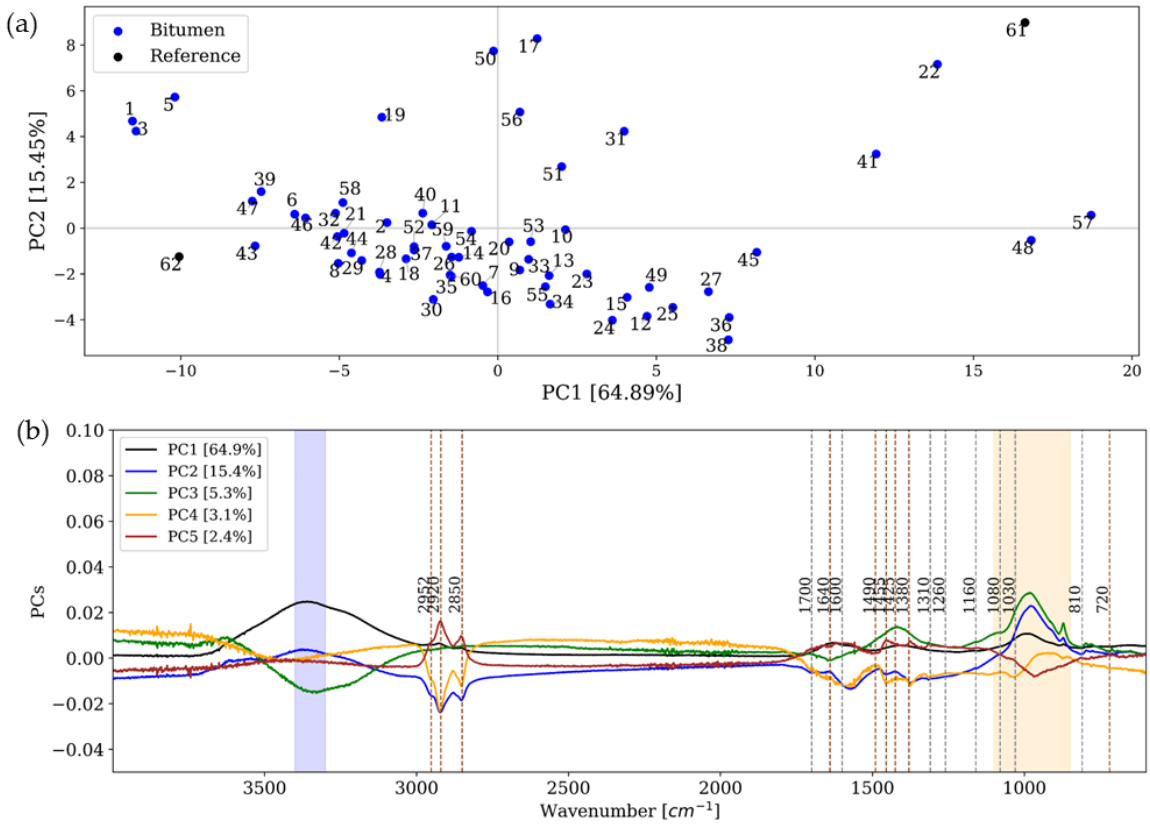

Figure 4. Score and loading plots from the principal component analysis (PCA) based on the Fourier transform infrared spectroscopy (FTIR) dataset in the range of 4000–400 cm^{-1}. (**a**) 2D scatter plot principal component 1 (PC1) and principal component 2 (PC2). Samples of bitumen analysed are indicated in blue, while reference samples, n.61 for the excavation soil and 62 for modern bitumen samples are shown in black. (**b**) Loading plot principal component 1 (PC1)–principal component 5 (PC5). Matrix entries: 60 × 14,935. The blue-shaded region indicates hydrogen-bonded –OH groups (resins, asphaltenes, and oxidation products), while the yellow-underlined area represents carbonate minerals, contamination, and fillers (Table 1).

PC1, which explains the most variance, accounts for 64.4% and is associated with inorganic contribution. It shows significant positive loading at around 3300–3400 cm^{-1} which corresponds to the intermolecular H bonds (-OH), indicative of ageing [34–36]. Additionally, the band attributed to carbonates and silicates at 1057 and 875 cm^{-1} is highlighted in brown. PC2 accounts for 15.4% of the variance and shows negative loading except for in the carbonates and silicates spectral region. PC3 explains 5.3% of the variance and exhibits positive loading in the range of 1500–1200 cm^{-1}, associated with aliphatic deformation [34–38] and in the carbonates and silicates spectral region. PC4 accounts for 3.1% of the variance and shows negative bands in the range of 1500–1200 cm^{-1}, associated with aliphatic deformation. Finally, PC5 contributes 2.4% of the variance and highlights the bitumen fingerprint characterised by a double-band typical shape in the range of 3000–2700 cm^{-1} and 1100–1500 cm^{-1}, here associated with pure bitumen [34–45].

Following dimensionality reduction via PCA, a robust machine learning model was applied to classify the bitumen samples based on their FTIR spectral profiles. The classifier was trained on the spectra associated with labelled archaeological samples collected in the Abu Tbeirah archaeological context and then applied to the "Undetermined" bitumen samples to predict their most likely class labels. Results are reported in Figure 5 where the training dataset is reported by small circles (for a total of n. 36 bitumen samples) while the test dataset (composed of n. 26 bitumen samples) is reported as large circles. Four distinct categories were established for the analysis: assigned Droplet-shaped artefacts (samples 2, 9, 22, 23, 32, 34, 36), Flat fragments (samples 10, 19, 38, 39, 51, and 52), Adhesives (samples 1, 37, 40, 43, and 47), and Ingots (five samples: 6, 35, 42, 44, and 46). The spatial distribution in PCA + SVM demonstrates a good consistency. Classification of the unknown analysed samples based on a support vector machine (SVM) is reported in Table 3.

Table 3. Summary of classification results for the unknown test samples. The table reports the sample ID, the predicted class, and the probabilities associated with the top-ranked classes.

Sample ID	Predicted Class	Predicted Class Probability	Maximum Probability Class	Maximum Probability
3	Adhesives	0.072	Droplet-shaped artefact	0.251
4	Ingot	0.094	Droplet-shaped artefact	0.177
5	Adhesives	0.080	Droplet-shaped artefact	0.243
7	Droplet-shaped artefact	0.170	Adhesives	0.183
8	Ingot	0.070	Droplet-shaped artefact	0.203
12	Flat fragment	0.082	Droplet-shaped artefact	0.199
13	Droplet-shaped artefact	0.133	Adhesives	0.188
14	Droplet-shaped artefact	0.190	Adhesives	0.184
15	Droplet-shaped artefact	0.128	Adhesives	0.177
16	Droplet-shaped artefact	0.171	Adhesives	0.182
17	Flat fragment	0.102	Droplet-shaped artefact	0.226
18	Ingot	0.090	Adhesives	0.180
20	Droplet-shaped artefact	0.163	Adhesives	0.190
24	Droplet-shaped artefact	0.174	Ingot	0.183
25	Droplet-shaped artefact	0.111	Ingot	0.187
27	Droplet-shaped artefact	0.175	Ingot	0.187
29	Ingot	0.077	Droplet-shaped artefact	0.183
31	Flat fragment	0.088	Ingot	0.204
45	Droplet-shaped artefact	0.154	Ingot	0.202
48	Droplet-shaped artefact	0.175	Ingot	0.192
50	Flat fragment	0.070	Droplet-shaped artefact	0.233
53	Flat fragment	0.080	Droplet-shaped artefact	0.201
54	Ingot	0.099	Adhesives	0.182
57	Droplet-shaped artefact	0.193	Ingot	0.187
59	Ingot	0.098	Droplet-shaped artefact	0.217
60	Droplet-shaped artefact	0.182	Adhesives	0.182

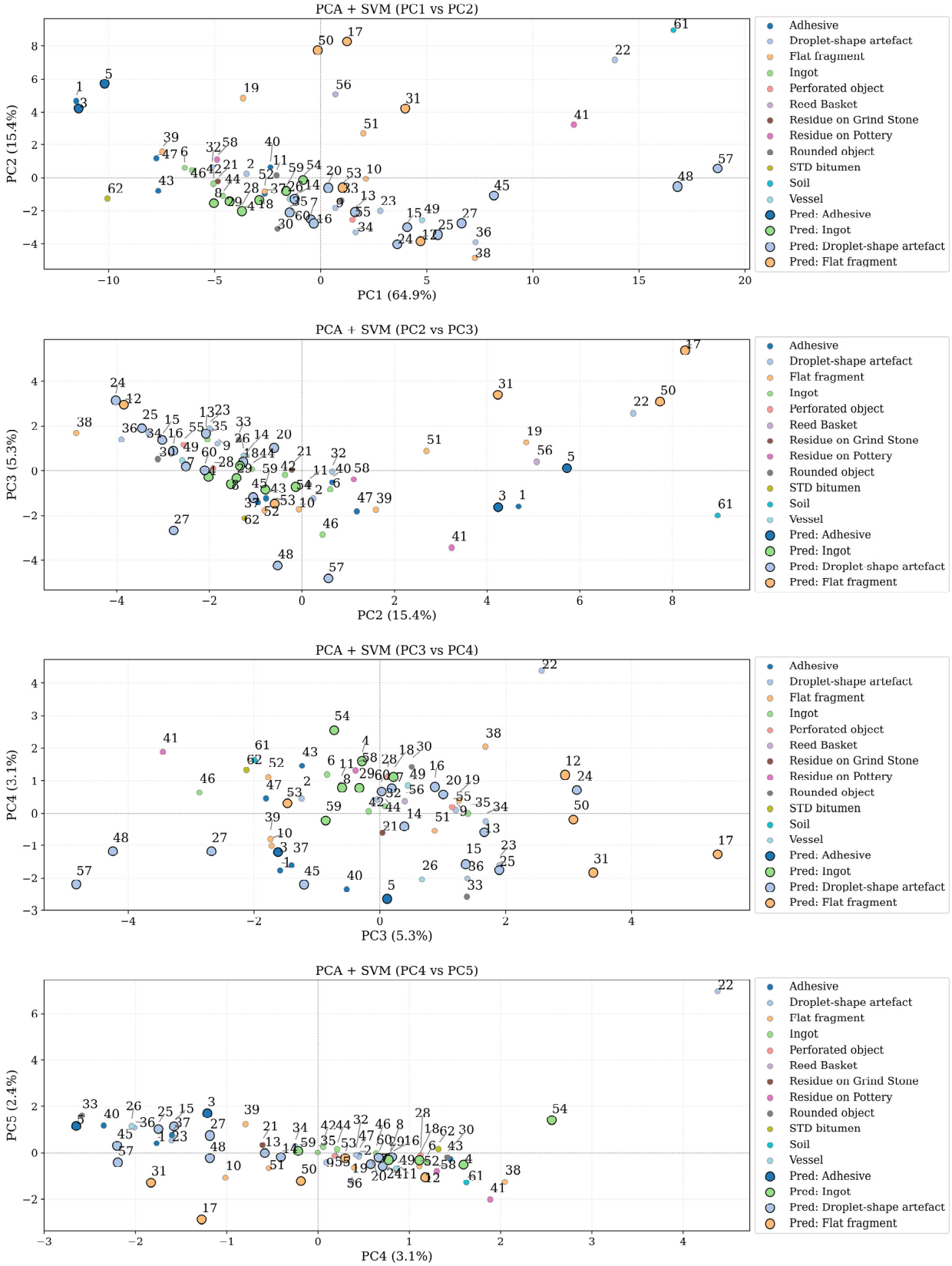

Figure 5. Principal component analysis (PCA) + support vector machine (SVM) model. Unknown samples are projected into the PCA space alongside known ones, giving a clear visual check of clustering and class confidence. Total labels: 62, known (training): 36, and unknown (test): 26. The metrics of such predicted classes and the probabilities associated with the top-ranked classes are reported in Table 3.

Notably, the adhesives reported as orange dots are in the IV quadrant of the PC1-PC2 plot and samples n. 3 and 5 have a similar composition to the adhesives, which are compatible from an archaeological point of view. Indeed, although these samples are not clearly identifiable as bitumen used as adhesive from their archaeological context, their chemical composition suggests that the material could potentially have been a product similar to adhesives. Ingots reported as green dots exhibit the best grouping along PCs and suggested a homogeneous composition with a low presence of additives. The Droplet-shaped artefact and Flat fragment samples display greater variance along the principal components, indicating a broader range of compositional variability within these classes. Our analytical approach has identified several samples as Predicted Ingots, indicating that their spectroscopic profiles closely match those of the known ingot samples. The predicted ingots samples n. 4, 8, 18, 29 come from a domestic context (Buildings A and D) whereas sample 54 was likely accidentally deposited in a grave backfill that cut into the earlier workshop area. Sample 59, by contrast, is directly associated with the workshop. The Predicted Droplet-shaped artefacts have spectral signatures that group them along PC2-PC3 and PC4-PC5. From an archaeological point of view, samples 7, 15, and 60 were recovered from Building D, samples n. 13, 14, 16, 24, 27, 48, and 57 were collected from Building A (the last two from the workshop), and sample 45 was collected from a funerary context. This recurring presence in domestic contexts confirms bitumen's likely use in common household items or activities. Since drop-shaped artefacts are hypothesised to have served as temporary storage forms—several having been found in a pit within a Phase 2 room of Building A—their marked compositional variability, combined with similarities to fragments and artefacts of different typologies, points to a continuous recycling process. This practice, with the exception of ingots and adhesives, likely involved mixing available bitumen of various origins and preserving it in such shapes for later reuse.

The Droplet-shaped artefact class is frequently predicted, but seldom with high confidence. Adhesive and Ingot often appear among the top three predicted probabilities. The training accuracy is 47.22%, meaning that the model correctly predicted the category for about 47% of the samples it was trained on (Table 4).

Table 4. Classification report (training set).

	Precision	**Recall**	**f1-Score**	**Support**
Droplet-shaped artefact	0.42	0.71	0.53	7
Flat fragment	0.67	0.67	0.67	6
Adhesive	0.80	0.80	0.80	5
Ingot	0.31	0.80	0.44	5
Accuracy	-	-	0.47	36
Macro avg	0.18	0.25	0.20	36
Weighted avg	0.35	0.47	0.39	36

The efficacy of the classification model is detailed in the accompanying confusion matrix (Figure 6). In this visualisation, each row corresponds to the actual class (ground truth), and each column represents the predicted class determined by the model. The numbers in each cell indicate the count of samples. The principal diagonal elements record the number of true positives, signifying the samples correctly classified for each class. The off-diagonal entries quantify the misclassifications.

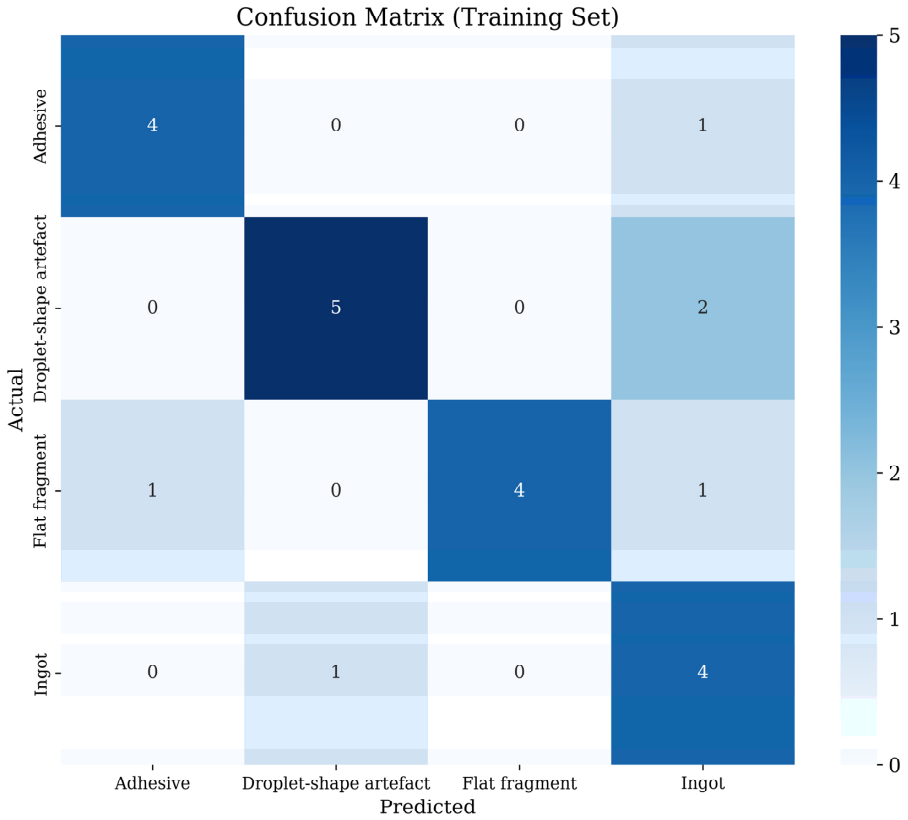

Figure 6. Confusion matrix (training set).

Looking at the FTIR spectra across the defined sample classes in Figure 7, it is shown that the Droplet-shaped artefacts and ingots exhibit the highest degree of spectral similarity while the Flat fragments display greater spectral variability. Specifically, it is noted that certain spectra, particularly those corresponding to samples 12 pred, 38, and 50 pred, lack the characteristic features attributable to the $n_{sym\&asym}CH$ stretching vibrations. Regarding Adhesives, sample 1 samples of a flint blade with a bitumen haft shows a low concentration of organic components.

The classification ranging from Adhesives—Ingots—Droplet-shaped artefacts—to Flat fragments represents a gradient from most pure bitumen to most filler presence, connecting the macroscopic shape and archaeological function with the microscopic structure of the samples. The classes named Adhesive and Ingot are more homogeneous. This finding not only allows for the confident identification of undetermined samples with similar compositional profiles but also carries significant archaeological implications. This homogeneity suggests that these categories might correspond to a specific recipe or standardised preparation method used by Sumerians. This observation aligns with the archaeological data from Abu Tbeirah, where ingot-shaped bitumen artefacts—characterised by flat bases with mat impressions—appear to have functioned as transport or storage units, possibly for standardised distribution. Similarly, fragments classified as Adhesives derive from contexts where bitumen was used as an adhesive, particularly for hafting tools or sealing containers, indicating specific preparation methods tailored to functional needs. Moreover, cuneiform sources refer to distinct types of bitumen—solid and liquid—likely corresponding not only to different intended uses (e.g., coating, sealing, and hafting) and modes of transport and storage, but also to intentionally differentiated compositions. Solid bitumen may have circulated in shaped forms such as ingots, while liquid bitumen was likely transported in containers such as jars, suggesting distinct chaînes opératoires and preparatory recipes adapted to functional and logistical needs. This aligns with archaeo-

logical evidence suggesting sophisticated material knowledge and specialised production processes in ancient Mesopotamia, where bitumen was a vital resource [32,46]. The recurrence of compositionally similar samples across different areas of the site, including but not limited to domestic contexts, indicates the use of specific bitumen formulations in routine tasks such as sealing containers, mending tools, or small-scale waterproofing. The Droplet-shaped artefacts proved to be less homogeneous in their composition, which suggests that these fragments may not represent a standardised product. Instead, they may represent residues or by-products from different phases of bitumen reworking, potentially reflecting transitional stages within broader recycling sequences. Their morphological similarity may be related to their function as single-use portions, set aside in preparation for subsequent recycling. Similarly, the Flat fragment, which lack a clear archaeological definition in existing literature, also exhibited low homogeneity. This suggests that they too may correspond to intermediate forms within the recycling process—material shaped or set aside for remelting, but not yet fully reintegrated into a functional product.

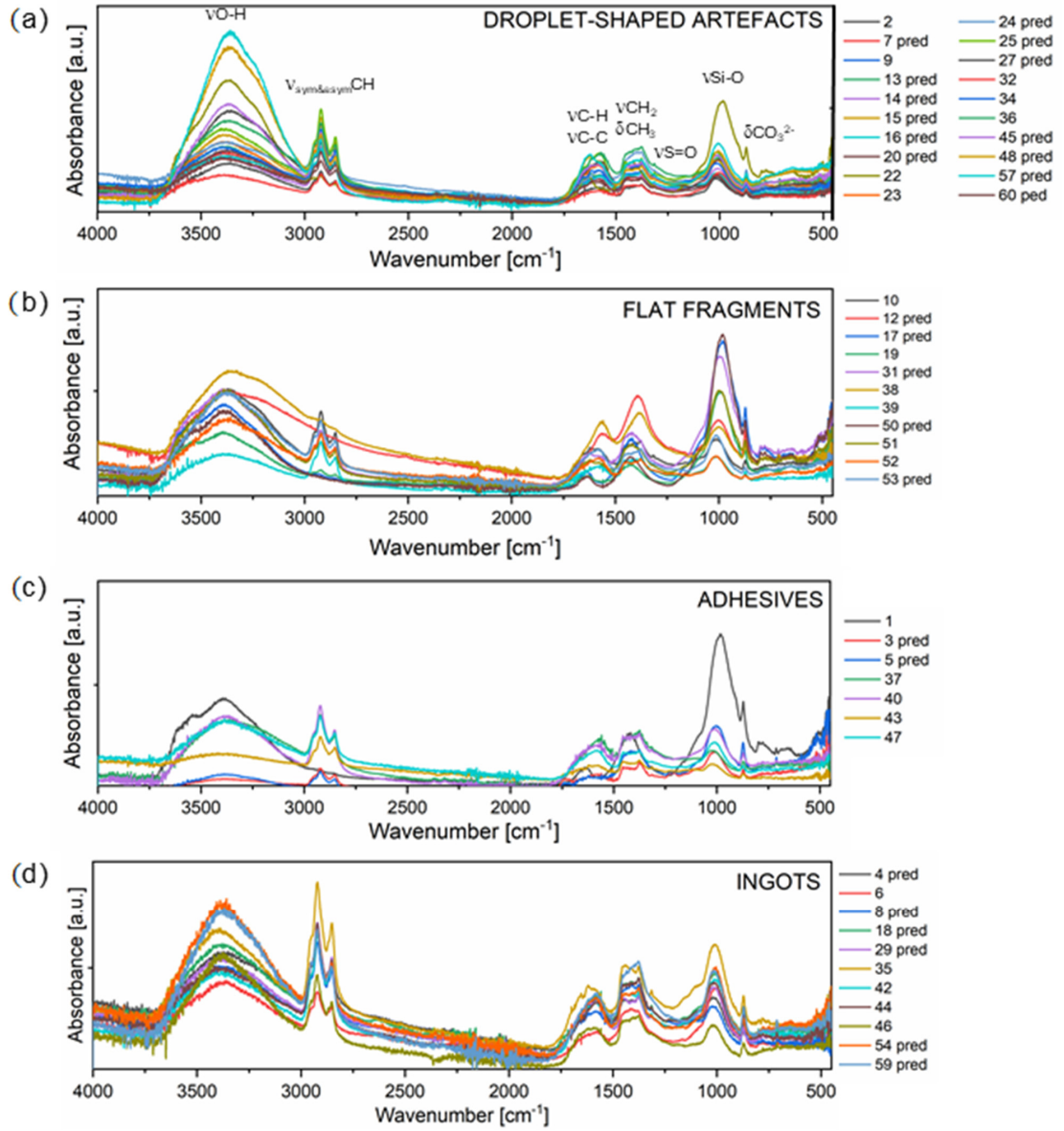

Figure 7. FTIR spectra of the samples grouped by classes: (**a**) Droplet-shaped artefacts, (**b**) Flat fragments, (**c**) Aadhesives and (**d**) Iingots.

4. Conclusions

A collection of 60 bitumen artefacts from the 3rd millennium BC Sumerian site of Abu Tbeirah (Iraq) was studied via FTIR and machine learning to unveil ancient working methods used for the repair, reuse, and recycling of everyday objects. The FTIR spectra showed significant chemical variations, which are attributed to different organic/inorganic content ratios and states of production. Characteristic spectral features were identified within the 1200 to 1800 cm^{-1} range, where the presence of bands associated with alkyl functional groups (sym. and asim. CH, -CH_2, and -CH_3) confirms the hydrocarbon matrix of the samples. Through the principal component analysis, PC1 is associated with inorganic contribution, showing significant positive loading of around 3300–3400 cm^{-1} corresponding to the intermolecular H bonds (-OH) indicative of ageing and the carbonates and silicates bands at 1057 and 875 cm^{-1}. PC2 shows negative loading except for in the carbonates and silicates spectral region. PC3 exhibits positive loading in the range 1500–1200 cm^{-1} associated with aliphatic deformation and in the carbonates and silicates spectral region. PC4 shows negative bands in the range 1500–1200 cm^{-1} associated with aliphatic deformation. PC5 highlights the bitumen fingerprint characterised by a double-band typical shape in the range of 3000–2700 cm^{-1} and the range of 1100–1500 cm^{-1}, here associated with pure bitumen. The kernel-based support vector machine (SVM) model, trained on archaeologically labelled samples, successfully predicted the classification of the undetermined samples, which comprised 30% of the dataset. The resulting spatial distribution in the PCA-SVM plot demonstrated high consistency, establishing a compositional gradient linked to the macroscopic observations: from the relatively pure bitumen found in Adhesives and Ingots, to the highly altered Drop and Flat fragment. The homogeneity observed in the spectral profiles of the Ingots and Adhesives is particularly noteworthy, suggesting that these materials may have corresponded to standardised recipes or specific preparation methods employed by the Sumerians.

Finally, this interdisciplinary methodology, combining archaeological classification with advanced analytical techniques and machine learning, offers a substantial contribution to the study of bitumen in Sumerian contexts, enhancing our understanding of technological knowledge, resource management, and the material dimension of daily life in third-millennium BCE southern Mesopotamia.

Author Contributions: G.F.: Conceptualisation, methodology, investigation, visualisation, project administration, supervision, data curation, discussion, formal analysis, and writing—original draft. C.S.: Conceptualisation, methodology, investigation, software and script development, discussion, and writing—review and editing. V.C.: Literature review, investigation, discussion, and writing—review and editing. S.G.: Investigation, discussion, and writing—review and editing. L.F.: Archaeological classification, discussion, and writing—review and editing. F.M.: Archaeological classification, discussion, and writing—review and editing. A.G.: Philological investigation, discussion, and writing—review and editing. A.T.: Archaeological classification, discussion, and writing—review and editing. L.R.: Conceptualisation, archaeological methodology and supervision, project administration, and writing—review and editing. All authors have read and agreed to the published version of the manuscript.

Funding: This research has been supported by the Italian Ministerial grant PRIN 2021 titled SLOW SUMER. Repair, Reuse, Recycling and Southern Mesopotamian Society in the Changing World of 2500-2000 BC, Project code 2022LFKPNH, CUP MASTER-B53D23001740006.

Data Availability Statement: The data is available upon request from the corresponding author.

Conflicts of Interest: The authors declare no conflicts of interest.

References

1. Connan, J. Use and trade of bitumen in antiquity and prehistory: Molecular archaeology reveals secrets of past civilizations. *Philos. Trans. R. Soc. Lond. Ser. B Biol. Sci.* **1999**, *354*, 33–50. [CrossRef]
2. Griffiths, G.; Langridge, R.; Cather, B.; Doran, D. Bituminous Materials. In *Construction Materials Reference Book*; Routledge: Abingdon, UK, 2013; pp. 393–420.
3. Bustillo Revuelta, M. Bituminous materials. In *Construction Materials: Geology, Production and Applications*; Springer International Publishing: Cham, Switzerland, 2021; pp. 401–434.
4. Langejans, G.; Aleo, A.; Fajardo, S.; Kozowyk, P. Archaeological adhesives. In *Oxford Research Encyclopedia of Anthropology*; Oxford University Press: Oxford, UK, 2022.
5. Colombini, M.P.; Modugno, F. *Organic Materials in Art and Archaeology*; John Wiley and Sons, Ltd.: Chichester, UK, 2009; pp. 3–36.
6. Woodside, A.R. Aggregates and fillers. In *Asphalt Surfacing*; Cambridge University Press: Cambridge, MA, USA, 1998; pp. 18–46.
7. Khan, N.; Karim, F.; Latif Qureshi, Q.B.A.I.; Mufti, S.A.; Rabbani, M.B.A.; Khan, M.S.; Khan, D. Effect of fine aggregates and mineral fillers on the permanent deformation of hot mix asphalt. *Sustainability* **2023**, *15*, 10646. [CrossRef]
8. Chen, C.W. A Mineralogical Approach to use the Non-qualified Fine Aggregates in Asphalt Concrete Pavement. Ph.D. Thesis, Université Paris-Est, Créteil, France, 2016.
9. Romano, L.; D'Agostino, F. (Eds.) *Abu Tbeirah Excavations, I. Area 1: Last Phase and Building A—Phase 1*; Sapienza Università Editrice: Rome, Italy, 2019; Volume 44.
10. Houhou, R.; Bocklitz, T. Trends in artificial intelligence, machine learning, and chemometrics applied to chemical data. *Anal. Sci. Adv.* **2021**, *2*, 128–141. [CrossRef] [PubMed]
11. Festa, G.; Christiansen, T.; Turina, V.; Borla, M.; Kelleher, J.; Arcidiacono, L.; Cartechini, L.; Ponterio, R.C.; Scatigno, C.; Senesi, R. Egyptian metallic inks on textiles from the 15th century BCE unravelled by non-invasive techniques and chemometric analysis. *Sci. Rep.* **2019**, *9*, 7310.
12. Scatigno, C.; Teodonio, L.; Di Rocco, E.; Festa, G. Spectroscopic Benchmarks by Machine Learning as Discriminant Analysis for Unconventional Italian Pictorialism Photography. *Polymers* **2024**, *16*, 1850. [CrossRef]
13. Festa, G.; Maggio, M.S.; Teodonio, L.; Scatigno, C. Ancient handwriting attribution via spectroscopic benchmarks and machine learning: 'Clavis Prophetarum' by Antonio Viera. *Expert Syst. Appl.* **2023**, *227*, 120328. [CrossRef]
14. Zhang, W.; Kasun, L.C.; Wang, Q.J.; Zheng, Y.; Lin, Z. A review of machine learning for near-infrared spectroscopy. *Sensors* **2022**, *22*, 9764. [CrossRef]
15. Lansford, J.L.; Vlachos, D.G. Infrared spectroscopy data-and physics-driven machine learning for characterizing surface microstructure of complex materials. *Nat. Commun.* **2020**, *11*, 1513. [CrossRef]
16. Meza Ramirez, C.A.; Greenop, M.; Ashton, L.; Rehman, I.U. Applications of machine learning in spectroscopy. *Appl. Spectrosc. Rev.* **2021**, *56*, 733–763. [CrossRef]
17. Vermeulen, M.; McGeachy, A.; Xu, B.; Chopp, H.; Katsaggelos, A.; Meyers, R.; Alfeld, M.; Walton, M. XRFast a new software package for processing of MA-XRF datasets using machine learning. *J. Anal. At. Spectrom.* **2022**, *37*, 2130–2143. [CrossRef]
18. Kim, J.J.; Ling, F.T.; Plattenberger, D.A.; Clarens, A.F.; Peters, C.A. Quantification of mineral reactivity using machine learning interpretation of micro-XRF data. *Appl. Geochem.* **2022**, *136*, 105162. [CrossRef]
19. Jetybayeva, A.; Borodinov, N.; Ievlev, A.V.; Haque, M.I.U.; Hinkle, J.; Lamberti, W.A.; Meredith, J.C.; Abmayr, D.; Ovchinnikova, O.S. A review on recent machine learning applications for imaging mass spectrometry studies. *J. Appl. Phys.* **2023**, *133*, 020702. [CrossRef]
20. Verbeeck, N.; Caprioli, R.M.; Van de Plas, R. Unsupervised machine learning for exploratory data analysis in imaging mass spectrometry. *Mass Spectrom. Rev.* **2020**, *39*, 245–291. [CrossRef] [PubMed]
21. Beck, A.G.; Muhoberac, M.; Randolph, C.E.; Beveridge, C.H.; Wijewardhane, P.R.; Kenttamaa, H.I.; Chopra, G. Recent developments in machine learning for mass spectrometry. *ACS Meas. Sci. Au* **2024**, *4*, 233–246. [CrossRef]
22. Fu, Y.; Shi, K.; Xi, L. Artificial intelligence and machine learning in the preservation and innovation of intangible cultural heritage: Ethical considerations and design frameworks. *Digit. Scholarsh. Humanit.* **2025**, *40*, 487–508. [CrossRef]
23. Towarek, A.; Halicz, L.; Matwin, S.; Wagner, B. Machine learning in analytical chemistry for cultural heritage: A comprehensive review. *J. Cult. Herit.* **2024**, *70*, 64–70. [CrossRef]
24. Fiorucci, M.; Khoroshiltseva, M.; Pontil, M.; Traviglia, A.; Del Bue, A.; James, S. Machine learning for cultural heritage: A survey. *Pattern Recognit. Lett.* **2020**, *133*, 102–108. [CrossRef]
25. Harth, A. The study of pigments in cultural heritage: A review using machine learning. *Heritage* **2024**, *7*, 3664–3695. [CrossRef]
26. Kennedy, C.J.; Penman, M.; Watkinson, D.; Emmerson, N.; Thickett, D.; Bosché, F.; Forster, A.M.; Grau-Bové, J.; Cassar, M. Beyond heritage science: A review. *Heritage* **2024**, *7*, 1510–1538. [CrossRef]
27. D'Agostino, F.; Kadhem, A.; Romano, L.; Vidale, M.; Angelozzi, M. Abu Tbeirah. Preliminary Report of the First Campaign (January–March 2012). *Riv. Degli Studi Orient.* **2011**, *84*, 17–34.

28. Jotheri, J.; Romano, L.; D'Agostino, F. *The Environment and Landscape Archaeology of the Abu Tbeirah Region*; Sapienza Università Editrice: Rome, Italy, 2019; pp. 49–53.
29. Forti, L.; Romano, L.; Celant, A.; D'Agostino, F.; Di Rita, F.; Jotheri, J.; Magri, D.; Mazzini, I.; Tentori, D.; Milli, S. The paleoenvironment and depositional context of the Sumerian site of Abu Tbeirah. *Quat. Res.* **2022**, *110*, 165–183. [CrossRef]
30. D'Agostino, F.; Greco, A. Abu Tbeirah. A philological and epigraphic point of view. In *Abu Tbeirah. Excavations I. Area 1. Last Phase and Building A-Phase 1*; Sapienza University of Rome: Rome, Italy, 2019; pp. 465–477.
31. Schwartz, M.P.; Hollander, D.J. Annealing, Distilling, Reheating and Recycling: Bitumen Processing in the Ancient Near East'. Paléorient, 26, 2, La Pyrotechnologie a ses debutes. Évolution des premieres industries faisant usage du feu/Early pyrotechnology. The evolution of the first fire-using industries. *Paléorient* **2000**, *26*, 83–91.
32. Available online: https://www.thermofisher.com/order/catalog/product/INQSOF018 (accessed on 28 July 2020).
33. Available online: https://www.originlab.com (accessed on 28 July 2020).
34. Ma, L.; Varveri, A.; Jing, R.; Erkens, S. Chemical characterisation of bitumen type and ageing state based on FTIR spectroscopy and discriminant analysis integrated with variable selection methods. *Road Mater. Pavement Des.* **2023**, *24* (Suppl. S1), 506–520. [CrossRef]
35. Hung, A.M.; Fini, E.H. Absorption spectroscopy to determine the extent and mechanisms of aging in bitumen and asphaltenes. *Fuel* **2019**, *242*, 408–415. [CrossRef]
36. Li, Z.; Fa, C.; Zhao, H.; Zhang, Y.; Chen, H.; Xie, H. Investigation on evolution of bitumen composition and micro-structure during aging. *Constr. Build. Mater.* **2020**, *244*, 118322. [CrossRef]
37. Hou, X.; Lv, S.; Chen, Z.; Xiao, F. Applications of Fourier transform infrared spectroscopy technologies on asphalt materials. *Measurement* **2018**, *121*, 304–316. [CrossRef]
38. Mirwald, J.; Werkovits, S.; Camargo, I.; Maschauer, D.; Hofko, B.; Grothe, H. Understanding bitumen ageing by investigation of its polarity fractions. *Constr. Build. Mater.* **2020**, *250*, 118809. [CrossRef]
39. Lamontagne, J.; Dumas, P.; Mouillet, V.; Kister, J. Comparison by Fourier transform infrared (FTIR) spectroscopy of different ageing techniques: Application to road bitumens. *Fuel* **2001**, *80*, 483–488. [CrossRef]
40. Larkin, P. *Infrared and Raman Spectroscopy: Principles and Spectral Interpretation*; Elsevier: Amsterdam, The Netherlands, 2017.
41. Efimov, A.M.; Pogareva, V.G. IR absorption spectra of vitreous silica and silicate glasses: The nature of bands in the 1300 to 5000 cm^{-1} region. *Chem. Geol.* **2006**, *229*, 198–217. [CrossRef]
42. Pipintakos, G.; Ching, H.V.; Mühlich, U.; Soenen, H.; Van Doorslaer, S.; Sjövall, P.; Lu, X. Experimental validation of the dual-oxidation routes in bituminous binders. In Proceedings of the RILEM International Symposium on Bituminous Materials: ISBM Lyon, Lyon, France, 14–16 December 2020; Springer International Publishing: Cham, Switzerland, 2022; Volume 271, pp. 903–909.
43. Hajji, S.; Turki, T.; Boubakri, A.; Amor, M.B.; Mzoughi, N. Study of cadmium adsorption onto calcite using full factorial experiment design. *Desalination Water Treat.* **2017**, *83*, 222–233. [CrossRef]
44. Primerano, K.; Mirwald, J.; Lohninger, J.; Hofko, B. Characterization of long-term aged bitumen with FTIR spectroscopy and multivariate analysis methods. *Constr. Build. Mater.* **2023**, *409*, 133956. [CrossRef]
45. Motevalizadeh, S.M.; Mollenhauer, K.; Wetekam, J. FTIR spectroscopy and multivariate discriminant analysis for classifying bituminous mastics: Exploring aging states and mastic composition. *Constr. Build. Mater.* **2024**, *438*, 137188. [CrossRef]
46. Connan, J. Use and trade of bitumen in antiquity and prehistory: Molecular archaeology reveals secrets of a 'fossil' material. *Philos. Trans. R. Soc. Lond. Ser. B Biol. Sci.* **2008**, *363*, 1692448.